IOP Conference Series: Materials Science and Engineering

Effects of the off-axis layer on the tensile failure of carbon fiber reinforced polymer $[0/\theta]_{ns}$ laminates

IOP Conf. Series: Materials Science and Engineering **576** (2019) 012024 doi:10.1088/1757-899X/576/1/012024

Effects of the off-axis layer on the tensile failure of carbon fiber reinforced polymer $[0/\theta]_{ns}$ laminates

Xi Deng[1], Wen-Xue Wang[2] and Terutake Matsubara[2]

[1]Department of Aeronautics and Astronautics, Engineering School, Kyushu University, Motooka Nishi-ku Fukuoka 819-0395, Japan
[2]Research Institute for Applied Mechanics, Kyushu University, Kasuga, Fukuoka 816-8580, Japan

Abstract. Off-axis plies have a great influence on the tensile failure stress of carbon fiber reinforced polymer (CFRP) multidirectional laminate. Matrix cracks in the off-axis plies will cause negative effect on the layers, leading to fatal failure of the laminate. A microscale cohesive zone model is proposed to explore the influence of matrix cracks in the off-axis plies on the tensile failure of $[0/\theta]_{ns}$ laminates. Simulations of tensile failure of $[0/\theta]_s$ laminate were performed by varying the off-axis ply angle θ ranging from 15º to 90º and the cohesive properties to investigate the effects of off-axis plies to the failure of the laminates. Tensile tests of [0/θ]2s laminates with various off-axis ply angles were conducted to validate the simulations of microscale model. The simulation results with matrix cracking are in high agreement with the experimental results, illustrating the influence of off-axis plies on the tensile failure of $[0/\theta]_{ns}$ laminates.

1. Introduction

Carbon fiber reinforced polymer (CFRP) multi-directional laminates are widely used in recent years. The off-axis layers play an important role in the CFRP multidirectional laminates to improve the in-plane shear properties although the final failure of a CFRP multidirectional laminate under tension is always controlled by the failure of 0º layers which are parallel to the load direction. However, the matrix crack which easily occurs in the off-axis layers and propagates parallel to the fibers is the most commonly observed damage in the relatively low tensile load [1-2]. This damage usually causes negative effects on the laminate properties, and even leads to laminate failure indirectly. Therefore, the investigation of the effects of the off-axis layer with matrix cracking on the laminate failure is helpful to analyze the strength of the whole laminate.

According to previous studies, matrix cracks are largely observed in off-axial layers. The most commonly observed cracks always take place in 90º plies normal to uniaxial loading. To explain the failure mechanics, various failure models have been proposed to illustrate the matrix cracking generating on the total failure. Tohgo [3] used a 2-D simulation to investigate ply-cracking damage for cross-ply laminate. The results showed that transverse cracking damage in 90º plies was first propagated. Li et al. [4] proposed a damage representation for cracked laminates with matrix cracking in the direction parallel to the fibers, in which a damage growth law was also combined.

In this study, aiming at investigating the effects of the off-axis layer on the tensile strength and failure behavior of $[0/\theta]_{ns}$ laminates, numerical simulation of $[0/\theta]_s$ (n=1) using finite element method and tensile tests of $[0/\theta]_{2s}$ (n=2) were conducted. A three-dimensional microscale model is proposed, in which the transverse matrix cracking is modeled by cohesive zone model by using cohesive interface

elements. Different cohesive energy release rate (G_c) values are used to reveal the effect of the transverse cracking resistance of the matrix on the failure of the laminate. Moreover, tensile tests of $[0/\theta]_{2s}$ laminates with various off-axis layer angles were performed. The failure processes of laminates with various off-axis layer angles were investigated in situ by using a digital microscope (Keyence VHX-2000) and a long distance high performance zoom lens (Keyence VH-Z50L).

2. Numerical simulation

In the numerical simulation, for the sake of simplicity, a $[0/\theta]_s$ laminate was modeled. A common geometry of a $[0/\theta]_s$ laminate is depicted in Figure 1. As is shown in Figure 1, the matrix cracks always occurred in the off-axis plies and extended along the fiber direction.

According to the symmetry of the stacking sequence of the $[0/\theta]_s$ laminate, only half of the laminate is needed to be simulated. Meanwhile, based on the periodicity of the microscale structures of the $[0/\theta]_s$ laminate, the whole laminate can be simulated by a representative unit cell (RUC) at a microscale level [6-8], as seen in Figure 1. This microscale RUC is generated using a rhombohedral unit cell, and it is located at the internal region of the laminate. The initiation and extension of a matrix crack is modeled at the center of the off-axis layer in the RUC by using the cohesive interface element. Since the matrix crack plane is parallel to the fiber direction in the off-axis layer, two boundary surfaces of the RUC that carry tensile load are also taken to be parallel to the matrix crack plane so that periodic boundary conditions are easily applied to the RUC. In this way, this RUC is useful for investigating the influence of off-axis layer.

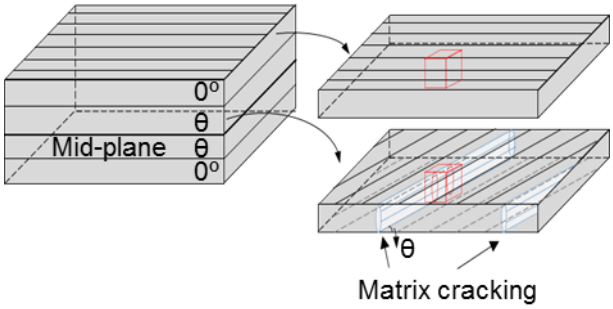

Figure 1. Sketch of $[0/\theta]_s$ laminate with matrix cracking.

The periodic boundary conditions must enforce the stress and displacement continuity between adjacent RUCs, and create the desired stress state in the RUC. In this way, the microscale model with the periodic boundaries is under same load condition as the whole laminate. For this reason, the periodic boundary conditions request the displacements of pair nodes in the corresponding surface should satisfy the relations of the displacements as follows [5]:

$$u_i^+ - u_i^- = \delta_i^* \quad i = x, y, z \tag{1}$$

where u_i^+, u_i^- denote the displacement components of pair nodes in the i-direction coordinate axis, δ_i^* means the stretch in the i-direction between the pair nodes on the corresponding surfaces. Applying the periodic boundary conditions to the RUC, the components of macroscopic tensile stress versus the tensile strain in this RUC can be calculated as follows:

$$\overline{\sigma_{ij}} = \frac{1}{V}\int \sigma_{ij}\, dV \tag{2}$$

where V is the volume of the microscale model.

The present finite element simulation was conducted by using MSC.Marc 2011. A three dimensional microscale model is shown in Figure 2. A single layer is 0.125 mm in thickness. The length of the microscale model varies with the off-axis angle θ, ranging from 0.618 mm to 0.4 mm for θ = 15º ~ 90º

to ensure the periodicity of the microscale model which includes a whole matrix crack. The width of the microscale model is 0.16 mm. In this microscale model, matrix, fibers and the cohesive elements are simulated separately and are described in different colors, respectively. One layer of the laminate includes three arrays of carbon fiber bundle, which is utilized to approximately simulate a single layer with fiber volume fraction of 60% according to the prepreg used in the fabrication of the laminates for the tensile tests. High order 10-nodes tetrahedral solid elements are adopted to make it better for simulating the plasticity of matrix and the failure of fibers. 6-nodes pentahedral cohesive elements are chosen to mimic the matrix crack initiation and propagation. In order to strike a balance between computational cost and simulation accuracy, the fibers in the laminate are assumed to be arranged in a square array and that the matrix cracks are uniformly spaced.

A general estimation of the total number of elements in such a microscale model is approximately 110000. In this microscale RUC model, the mesh of the microscale model is carefully constructed that the nodes on the pair corresponding surface are arranged with the same distribution. This mesh is used to ensure the application of periodic boundary conditions. Furthermore, the fiber and matrix nodes are also constructed to be coincident at the fiber-matrix interface, since this manner can greatly reduce numerical iteration cost in contact analysis along the surface. The possible debonding between fibers and matrix was not considered in the present simulation. Hence, the matrix cracking in the off-axis layer and fiber fracture are the main damages which cause the laminate failure.

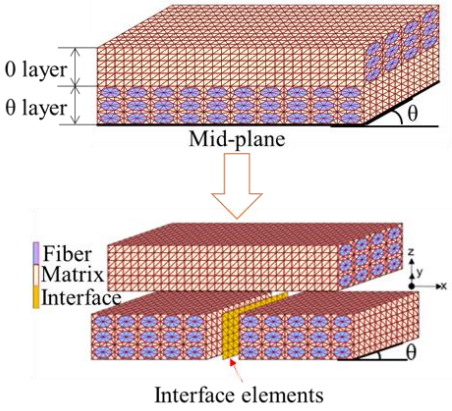

Figure 2. Description of the $[0/\theta]_s$ microscale model (in this figure, θ = 45º).

In the MSC.Marc, one of the ways to implement the periodic boundary conditions is to use the option "servo-link". This option allows to prescribe multi-point boundary conditions for nodal displacements expressed as a linear function with constant coefficients. The relation is described as follows [9]:

$$\mathrm{u} = a_1\mathrm{u}_1 + a_2\mathrm{u}_2 + \cdots \tag{3}$$

where u sis a degree of freedom to be constrained; u_i $(i = 1, 2, \cdots)$ are the other retained degrees of freedom in this structure; a_i $(i = 1, 2, \cdots)$ are constants provided in this option. With this option, the periodic boundary condition is easily applied to the microscale model.

The cohesive interface elements are inserted into the matrix region where the matrix crack may initiate. In principle, the matrix crack can be positioned anywhere within the matrix region in the microscale model. In this simulation, the crack position is located at the center of the microscale model, as shown in Figure 2. These cohesive interface elements simulate the onset and propagation of the matrix crack based on the cohesive zone model (CZM). The cohesive zone elements do not need to represent any physical material so that it can be modeled with an initial zero thickness, just as Figure 2 depicted. The properties of cohesive elements are defined by a bilinear curve, as is described in following Figure 3. The relations among the maximum critical traction T_c, the energy release rate G_c, the maximum

opening displacement δ_m, the critical opening displacementδ_c, and the initial stiffness K satisfy the following equations [9-10]:

$$\delta_m = 2G_c/\delta_c \tag{4}$$

$$\delta_c = T_c/K \tag{5}$$

Through the simulation of the cohesive elements, the matrix crack initiates if the cohesive energy reaches the critical energy release rate. After then the cohesive traction reduces, and as the traction reduced to zero, the cohesive zone disappears and the matrix crack occurs.

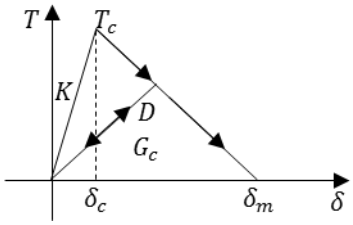

Figure 3. Bilinear curve of traction-displacement relation.

The material properties of the microscale model are defined separately. The matrix is considered as an elastic-plastic isotropic material, carbon fiber is defined as a transverse isotropic material, and the interface element is of zero-thickness, respectively. The material constants of matrix and fibers are listed in Table 1 and the constants of the cohesive interface element are listed in Table 2. To estimate the failure of the carbon fiber, the maximum stress criteria of the carbon fiber material are also listed in Table 1. The elastic-plastic property of the matrix is prescribed through a power law as follows [11]:

$$\sigma_m = A\left(\varepsilon_m^p\right)^r + \sigma_y \tag{6}$$

where A = 256, r = 0.259, σ_y = 30 (MPa) are employed in this simulation to approximately describe the relation between the equivalent plastic strain and the stress.

Table 1. Constants of materials

Constants	Carbon fiber	Matrix
E_1 (GPa)	235	3.3
E_2, E_3 (GPa)	13	
μ_{12}, μ_{13}	0.2	0.38
μ_{23}	0.3	
G_{12}, G_{13} (GPa)	15	1.2
G_{23} (GPa)	5	
σ_{t11} (MPa)	4936	
σ_{c11} (MPa)	2820	
τ_{12} (MPa)	700	

Table 2. Constants of cohesive elements

Constants	Value
Cohesive energy G_c (N/mm)	0.001~0.4
Critical opening displacement δ_c(mm)	$8*10^{-7}$
Maximum opening displacement δ_m (mm)	0.01
Stiffness of cohesive element (N/mm^3)	10^8

In order to investigate the effect of the off-axis layers on the failure of the laminate, microscale models with off-axis angle θ ranging from 15°~90° are simulated, respectively. The effect of off-axis layers on the global stress can be clarified easily by analyzing the failure stress with the variation of off-axis angle θ. Furthermore, more simulations were conducted with various cohesive energy release rate G_c to investigate the effect of fracture toughness of the matrix on the failure strength of the laminate.

Several cases of initially complete crack, crack-free, and those between these two ideal situations by altering cohesive energy release rate G_c of cohesive elements are simulated.

3. Tensile tests

Tensile tests were carried out to validate the availability of the proposed microscale model. However, the $[0/\theta]_s$ laminate is too thin that it is hard to handle during the tensile test because a small scratch may lead to large decrease on the failure strength. Therefore, $[0/\theta]_{2s}$ laminates are fabricated for the tensile tests. The off-axis angle of θ were chosen as 15º, 30º, 45º, 60º, 75º and 90º, respectively. T700S/2500 carbon fiber/epoxy prepreg (ply thickness $t_0 = 0.125$ mm) was used to fabricate the laminates. The carbon fiber volume fraction of the prepreg was 60%. Each laminate was cured at 135℃ for 2h by autoclave. The size of laminates was $250\text{mm} \times 250\text{mm} \times 1$ mm to ensure reliability of the experimental results, 9 specimens were fabricated for each $[0/\theta]_{2s}$ laminate. The specimen is 240 mm in length and 25 mm in width, respectively, as described in Figure 4. The end tabs have a thickness of 2 mm, length of 55 mm, and a slope of 5 mm.

In order to observe damage events such as matrix crack initiation, propagation and fiber breaking at the free edge of the specimen, one side section of each specimen is firstly grinded through 600#, 1500#, 2000#, 2500#, and 4000# sandpaper, and is secondly polished by 1 μm and then 0.06 μm Al_2O_3 powder. The surface failure processes of each specimen were monitored in situ using a digital microscope (Keyence VHX-2000) and a long distance high performance zoom lens (Keyence VH-Z50L) during the tensile test. In particular, at the three load levels of 30%, 50% and 80% of the average tensile strength of the laminate, the load state was held on and the detail surface damage modes were recorded by enlarged photographs. Matrix crack density was investigated based on the observation data. Tensile tests were conducted by using a MTS 810 materials testing system with 1 mm/ min. crosshead rate.

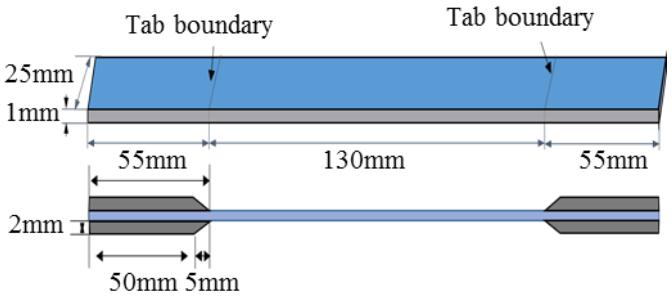

Figure 4. The size of the specimen in tensile tests.

4. Results and discussions

4.1. Numerical results

The variation of tensile failure strength of the laminate with the off-axis layer angle is presented in Figure 5 with the energy release rate of the matrix as parameter. The crack-free case indicates the microscale model without crack. In this case, no cohesive interface elements were inserted in the microscale model. With the off-axis angle increasing from 15º ~ 90º, the tensile failure stress decreases rapidly when the off-axis angle θ is smaller than 45º. After that, the tensile failure stress has relative small variation with the increase of the off-axis layer angle. A minimum value seems to exist in the range of $\theta = 60º \sim 75º$. A little increase trend is observed conversely as the θ increases to 90º. In the cases that adding the cohesive interface elements to simulate the matrix cracking, the variation of the tensile failure stress versus θ demonstrates similar tendency, except that the values of tensile failure stress of the laminate with matrix cracking is always smaller than that without matrix cracking. These results indicate that the off-axis angle has a significant effect on the failure of the $[0/\theta]_s$ laminate. The

case that $G_c = 0.001\ N/\text{mm}$ approximately simulate that the matrix crack exists initially in the microscale model.

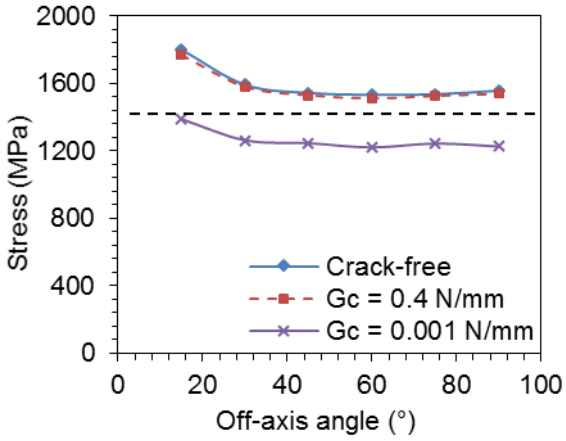

Figure 5. Relations of failure stress to off-axis angle.

The horizontal dash line plotted at the stress 1390 MPa represents the failure stress carried by only the 0º plies if the off-axis plies are assumed to be failed and cannot carry any load. Comparing this reference failure stress with those of failure stress of laminates with or without matrix cracking, it is observed that the off-axis layer always plays positive role if there is no crack in the off-axis layers. The tensile strength of the laminate with off-axis layer angle smaller than 45º is many higher than the reference failure stress. The tensile strength of the laminate with off-axis layer angle in the range of 45º ~ 90º is slightly higher than the reference failure stress. In the cases of small off-axis layer angle and high energy release rate, the off-axis layer still plays positive role and the tensile failure stress is still higher than the reference failure stress. However, in the cases of large off-axis layer angle and low energy release rate, the off-axis layer usually plays negative role and the tensile strength of the laminate is many lower than the reference failure stress. From these results, it is realized that off-axis layer angle and fracture toughness of the matrix have significant influence on the tensile strength of the multidirectional laminates.

4.2. Experimental results

The experimental results are plotted in Figure 6 ~ 8. The variation of averaged tensile strength of the laminate with the off-axis layer angle is presented in Figure 6. The tensile failure stress illustrated similar tendency with the numerical simulation results. The region above the horizon line means that the off-axis layer in laminate has positive effect on the tensile failure strength of the laminate. However, the off-axis layer show negative influence on the tensile strength of the laminate when the off-axis angle θ is in the range of 60º ~ 75º. Comparing the experimental curve with those simulation curves shown in Figure 5, the experimental curve agreed well with the case that $G_c = 0.4\ N/\text{mm}$, as is shown in Figure 6. The difference between two methods were due to the inexact assumptions and parameters in simulation. Therefore, to accurately predict the tensile strength of a laminate, correct energy release rate value of the matrix is necessary.

The typical in situ observation results of damage images on the free edge of each type laminate at the load level of 80% are described in Figure 7. Fiber breakage and matrix cracks were observed by the microscope. For the tensile load level of 30% in the tensile process, there was no damage found on the observing free edge of all the $[0/\theta]_{2s}$ laminates. As tensile load increased continuously to the tensile load level of 50%, fiber breakage initiated first in the 0º layers. The dashed open arrows plotted in Figure 7 referred to the fiber breakages in the laminates. On the other hand, there was still no matrix crack initiated in off-axis layers in this period.

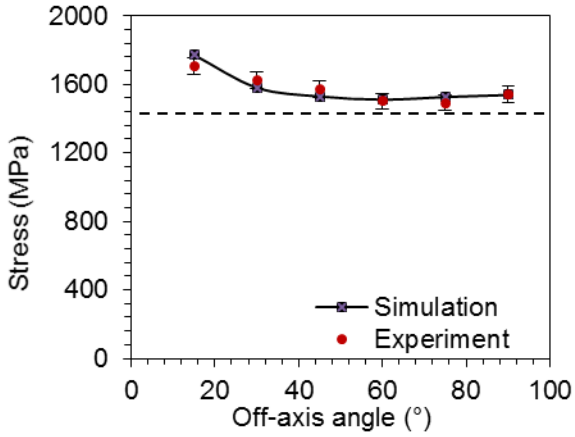

Figure 6. Experimental results of failure stress to off-axis angle. Dashed line indicates the assumed stress that off-axis layer cannot carry any load.

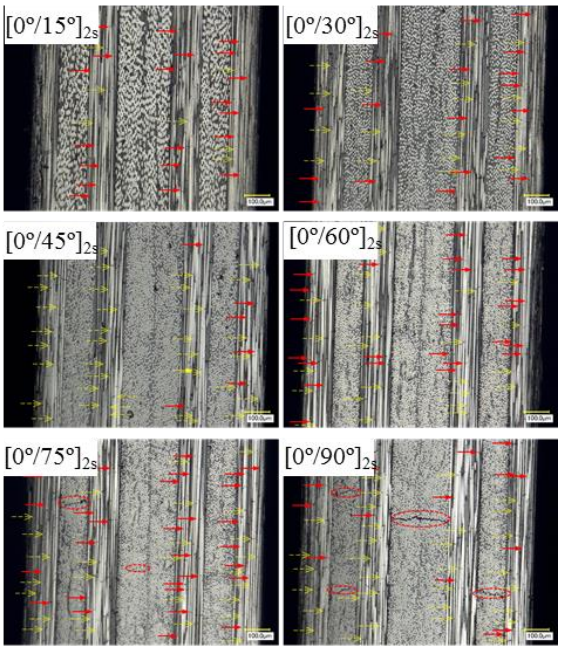

Figure 7. Failure modes of laminates under tension. Long dashed open arrows refer to the fiber breakages before 50% load, the solid arrows refer to new fiber breakages under 80% load, and the dashed circles marked the matrix cracks.

When the tensile load reached the level of 80%, new fiber breakages initiated intensively at the positions among the existing damages, accompanied with the propagation of previous existing fiber breakages. Solid arrows portrayed in Figure 7 pointed to the new fiber breakages developed at the load level of 80%. The number of the fiber breakage in 0º layers was almost saturated at this tensile load level. Meanwhile, matrix cracks were observed in two types of layups barely, which are the $[0/75º]_{2s}$ and $[0/90º]_{2s}$ laminates. The matrix cracks are signed by dashed circles in Figure 7. As this result, it indicated that the matrix cracks merely occurred in the laminate that the off-axis angle was larger enough.

According to the experimental results of all the $[0/\theta]_{2s}$ laminates, for the laminates with off-axis angle θ lower than 75º, the matrix crack did not occur in the specimens until the final tensile failure. For the

cases that the off-axis angle θ in $[0/\theta]_{2s}$ laminate reached 75º, as the off-axis angle increased, the matrix crack initiated under a smaller strain. Meanwhile, the matrix crack initiated and propagated more intensive in the $[0/\theta]_{2s}$ laminate with larger off-axis angle. The relations of matrix crack density in central off-axis layers to tensile strain are depicted in Figure 8. In addition, there is no interfacial delamination in all the specimens during the tensile tests, hence the effect of delamination is negligible.

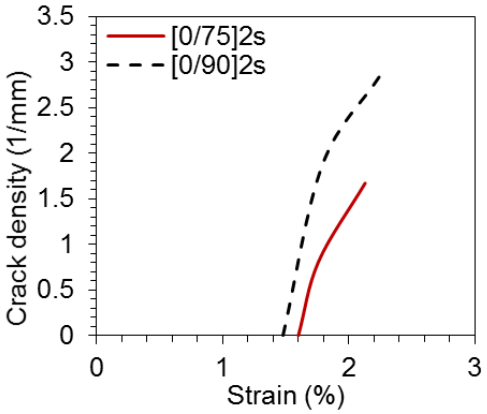

Figure 8. Relations of matrix crack density to failure strain.

5. Conclusions

The effect of off-axis layer on the failure of CFRP $[0/\theta]_{ns}$ laminates is investigated by finite element analysis and tensile tests of $[0/\theta]_{2s}$ laminates. Based on the present numerical and experimental results, the following conclusions are obtained.

1. The variation of off-axis angle leads to a reduction on the failure stress for most conditions. As the off-axial angle increases to 75º, the failure stress keeps decreasing directly. When θ>75º, A little increase is observed conversely as the θ increases to 90º.
2. Lower G_c of the matrix leads to low tensile failure stress. Comparing the numerical results to the reference stress, revealing the effect of the off-axis layer on the failure of the laminates intuitively.
3. Series of $[0/\theta]_{2s}$ specimens($15º \leq \theta \leq 90º$) were tested to validate the simulations. Matrix cracks and fiber breakages were observed to analyze the failure modes of laminates. Matrix cracks initiated merely in the laminate with large off-axis angle. The matrix crack density was higher in the laminate with large off-axis angle as well.

6. References

[1] Nairn J A 2001 *Polym. Matrix Compos.* **2** pp 1-33.
[2] Abrate S 1991 *Compos Eng.* **1** pp 337–53
[3] Tohgo K, Sugiyama Y and Akizuki K 2001 *JSME Int. J. Ser. A.* **44** pp 282-90.
[4] Li S, Reid S R, Soden P D 1998 *Phil. Trans. R. Soc. Lond. A.* **356** pp 2379-412.
[5] Drach A, Drach B and Tsukrov I 2014 *Adv. Eng. Softw.* **72** pp 18-27.
[6] Romanowicz M 2016 *Compos Part B.* **90** pp 45-57.
[7] Tran T, Kelly D, Prusty B G, Pearce G and Gosse J 2013 *Compos. Struct.* **103** pp 1-8.
[8] Ellyina F, Zhang YF and Xia ZH 2011 *Procedia Eng.* **10** pp 63-8.
[9] MSC Software. *MSC Marc 2011 User Documentation, Volume A : Theory and User Information* (2011).
[10] Vandellos T, Huchette C and Carrère N 2013 *Compos. Struct.* **105** pp 199-206.
[11] Sun C T and Chen J L 1991 *Compos. Sci. Technol.* **40** pp 115-29.